A Computational Study on the Aerodynamics of a 90 mm Ducted Contra-Rotating Lift Fan

Yangang Wang*, Weixiong Chen, Haitong Wang, and Ruiyu Li
School of Power and Energy, University of Northwestern Polytechnical University, Youyi WestStreet, Xi'an, P. R. China

ABSTRACT

In this paper, a steady 3D numerical study has been conducted on a 90 mm counter rotating lift fan to investigate its aerodynamic performance. The effect of axial distance between the fans and rotor speed are studied. A low thrust generation has been revealed from the simulation results due to the unfavourable working condition for the upstream rotor. Subsequently, an inlet guide vane (IGV) is geometrically designed to cause a pre-swirl effect at the inlet. Results show that the pressure ratio and total thrust are significantly improved at 10% by the IGV with a little sacrificing in efficiency. Such work can be a guidance in the further design and optimization.

Keywords: Contra-rotating lift fan; Rotation Speed; Axial Space; Pre-swirl

Nomenclature

C	blade chord length at hub
T_0	inlet total temperature
P_0	inlet total pressure
q_m	mass
β	flow angle
β_1	inlet flow angle
β_2	outlet flow angle
$\beta_1 k$	inlet metal angle
$\beta_2 k$	outlet metal angle
c	absolute flow velocity
u	rotation velocity
w	relative flow velocity
θ	rotation velocity
π_k*	total pressure ratio
α	attack angle

1 INTRODUCTION

Micro air vehicles (MAVs) are flying vehicles with a proposed small geometric dimensions, which has been fostered continuous research due to their potential applications in civilian and military. Existing MAVs can be briefly categorized into three different concepts: fixed, rotary and flapping wing. Fixed and out-rotary concepts has drawn a tremendous research in the past decades, which benefits from the conventional technologies. However, they have been observed to suffer from an unfavorable aerodynamics in minimizing the dimensional. Flapping wing MAVs, as the most intriguing type in MAV family are regarded as the most efficient prototype, while their difficulties in control and maneuver restrict its develop. Ducted fan MAV, as one special rotary MAV has obtained huge attention recently. The well documented advantage of the ducted fan MAV is its efficiency due to duct lip and enhanced blade tip lift. Moreover, the shrouded blades make such an MAV able to achieve a near wall mission and low noise production. The ducted fan submersed in the MAVs are normally driven by propellers or lift fans to perform a vertical/short takeoff and landing (VSTOL) capability. Instead of a single lift fan, the ducted fan aircrafts are normally equipped with contra-rotating fans [1, 2] in order to increase the net thrust and minimize the contra rotating torque which is suitable for a tailless configuration.

In view of the aerodynamics, the rear rotating fan refines the wake direction closer to the axial flow, and then enhance the performance [3]. The flow field of a contra-rotating ducted fan is extremely complex due to mutual aerodynamic interference effects of the high-speedy rotating fans. The aerodynamic of the rotors can significantly influence the overall performance of ducted fan MAVs. Relative studies are well documented in literatures. Guerrero et al.[4] proposed an aerodynamic prediction methodology that can be used for conceptual designing ducted-fan vertical takeoff and landing unmanned air vehicle. Their method is based on a parametric geometry model and semi-empirical aerodynamic methods, and the results were validated with wind tunnel test data on a full-scale vehicle. Williams et al.[5] performed the steady and unsteady aerodynamic studies on ducted fans using a frequency domain panel method based on three-dimensional linear compressible lifting surface theory. Their result shows that the duct has an adverse effect on the aero-elastic stability of the rotor. Page[6] developed a vortex blade-element propeller design and analysis procedure to the design and analysis of single- and counter-rotation ducted fans, which can be used on a single-rotation ducted fan with a fixed stator or a dual-rotation ducted fan. Stiltner et al.[7] performed a detailed design phase of a ducted fan MAV. With the detailed design phase completed, they moved forward with the construction of the MAV and improved some ways to fabricate the vehicle. Finally, tests including thrust testing, landing gear drop tests, electronic benchmarking and the beginning of tethered tests on the duct fan MAV were conducted on the constructed vehicle. Sharma[8, 9] investigated the influence

*Email address(es): wyg704@nwpu.edu.cn

of axial gap on the performance of upstream rotor combining a low-speed (maximum speed 2,500 r / min) test rig, their studies indicate that the axial gap between the rotors has an important impact on the performance, and thus affect the performance of the compressor. At a small axial clearance, the rear rotor can effectively delay the stall on the front rotor, however, they didnt made a detailed explanation of the flow mechanism. Later on, Wang et al.[10] continuously studied the effect of axial space between two blade rows, they indicated that the axial space can significantly affect the performance of fan, and it is always essential to optimize a critical space by trading off with the structure limitation.

Since 2013, our group from the School of Power and Energy in the Northwestern Polytechnical University has engaged in the research of ducted fan MAVs regarding the related technologies in aerodynamics, mechanism, electronics and autonomy, etc. A remote controlled ducted MAV (named as FanSO) driven by ducted lift fan has been developed recently, see in Figure1(a). The MAV is fabricated by balsa wood and Polylactide (PLA). It is 590 mm in length and 380 mm in height. Two batteries with the capacity of 5000mAh each can perform a 10 min flight duration. Figure 2(b) shows the details of the contra-rotating ducted lift fan equipped on the FanSO. The diameter of the hub and shroud is 36.4 mm and 90 mm, respectively. It is around 320 mm long. Two 12-blades fans are parallel mounted along the axis with a axial space around 22 mm. At working speed (RPM=26000), the lift fan can achieve maximal 25 Newton net lift and 3.5 kW power. Our purpose to obtain a deep understanding into the ducted fan flyer has triggered both experimental and computational studies. The experiences gained from the research activities will be used for further development and optimization. It is, however, realized from the free flight test that the commercially ordered lift fan cannot achieve an expected lift which inspires us to perform a study into the inner flow behavior.

In this paper, computation is conducted solely on the ducted lift fan isolated from the MAV to predict the aerodynamic characteristics of the lift fan. Effect of axial space, inlet/outlet metal angle and RPM are evaluated in terms of thrust production, energy consumption and efficiency. In addition, an inlet guide vane (IGV) is developed and introduced into the lift fan system which provides a considerable improvement in the thrust generation due to the pre-swirl effect. The present study will guide the further design and optimize of the ducted fan MAV.

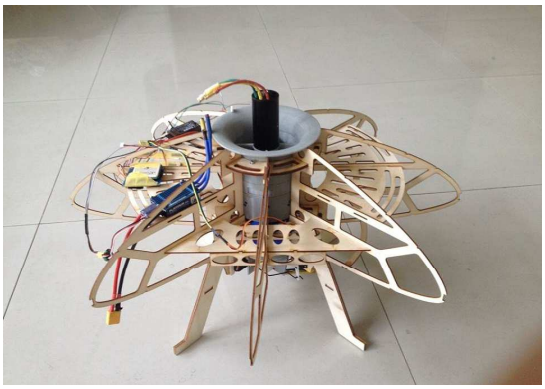

(a) NPU-1

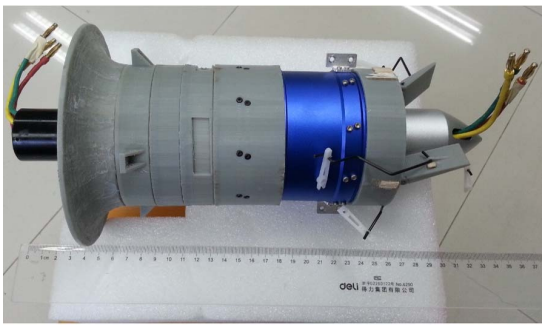

(b) Ducted Contra-Rotating Fan

Figure 1: NPU-1 and the ducted contra-rotating lift fan

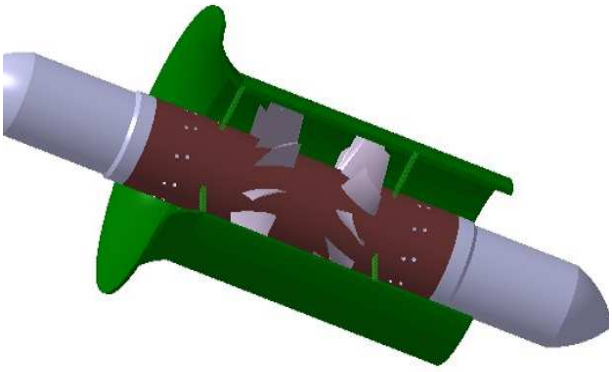

Figure 2: 3D topology of the ducted lift fan rendered in CATIA.

2 METHODOLOGY

The geometry of the fan blade is obtained by a 3D Laser scanning machine, which can resolve down to 0.02 mm. Figure 2 geometrically shows the schematics of the lift fan.

The commercial software NUMECA Autogrid was employed to generate the grid system of the lift fan. The blade and hub surface is meshed with Cartesian O and H mesh while the 3D space is filled with O4H type mesh, as shown in Figure 3. The butterfly grid was used for the tip clearance between the blade tip and the shroud. A refined y+ is set less than 2.0 at the nonslip and adiabatic wall boundary conditions for capture the boundary layer flow phenomena which results in 1.1 million cells in total. Note that only one passage is

meshed and computed, the entire flow field will be mirrored later on.

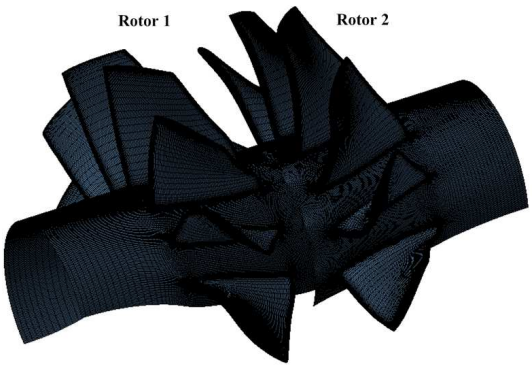

Figure 3: Grid system of the lift fan.

The steady simulation for the counter-rotating lift fan were performed using the flow solver EURANUS. It computed the conservative Reynolds Averaged Navier-Stokes (RANS) equations coupled with one equation Spalart-Allmaras (S-A) turbulent model which is widely used to investigate the effect of viscosity in turbomachinery. In our case, the Reynolds number of the counter-rotating lift fan is about half million. In the work of this paper, the mixing plane between two rows was treated using conservative coupling by pitch-wise rows approach, which was able to guarantee strict conservation of mass, momentum and energy through the interface of the two blade rows. The controlling equations are spatially discretized via a cell-centred finite volume formulation, for steady simulations, the equations were solved using an explicit four-order Runge-Kutta method with a local time step to obtain steady-state solution. The computational cost can be dramatically reduced by local time marching, implicit residual smoothing, and multi-grid techniques. The flow angle β, total pressure (P_{01}), and total temperature (T_{01}) are specified to be uniform across the whole inlet area in accordance to actual operation point, chock point. That means the inlet and outlet area were set as the local atmosphere condition (P_{01}= P_2=101325 Pa, T_{01}=288.15 K,). The performance curves were achieved by increasing the rotating speed at the chock point of the lift fan.

3 Aerodynamic Performance

3.1 Effect of Axial Space

Figure 4 depicts the influence of axial spacing on mass, pressure ratio, efficiency, thrust, power at design speed at 11 different axial spaces. It can be seen that the pressure ratio, axial thrust and power follow with an asymptotical likehood tendency and almost remain the same with the increasing axial space. The rotor1 efficiency almost remain the same with the increasing axial space while the rotor2 and total efficiency increased firstly and then decline along with the increasing axial space, where the maximal value (83.5% and 80%, respectively) peaks at 0.7c. It can be conjectured that at small axial space (say below 0.5), the upstream rotor wake at the exit cannot fully mixed with the mainstream, which results in an unfavorable incoming flow for the downstream rotor. When increase the axial space (say between 0.5-0.7), upstream wakes and mainstream can be fully mixed during the relative long distance, which provide an better incoming flow for the downstream rotor, hence, gives a higher efficiency ; Continuing increasing the axial space, mixing loss will predominate the flowfield, which leads to a decline of the efficiency.

3.2 Flow Angle Analysis

As known, the effective angle of attack can be derived from the difference between the inlet flow and metal angle, say $\alpha = \beta - \beta_k$. The preferable working condition happens at a positive angle of attack. Figure 5 plots the inlet/outlet flow and metal angles along the blade height for both upstream and downstream rotors. It can be seen from Figure 5(a) that the upstream rotor angle of attack turns lower gradually along the increase of blade height, and the AOA turns to negative when the radius is more than about 30% of the blade span. It means that the load magnitude of rotor decrease gradually along the blade height, which can explain the low total pressure at the upstream rotor. Meanwhile, negative AOA will bring greater pressure loss due to boundary layer on pressure surface, which can explain the low efficiency at the upstream rotor. The angle distribution of the downstream rotor performs a similar behavior to the upstream rotor which can be revealed from Figure 5(b). However, due to contra-rotating effect, the downstream rotor works at a positive angle before 65% blade span, and the difference is very small even though the AOA after 65% blade span is negative, which results in a larger turning angle of airflow and improves the working capacity of the downstream rotor. The loss level is also relatively less than the upstream rotor, so as to retain high efficiency and gain greater thrust. In addition, by looking into Figure 5, the blades are mostly working at high angle of attack either in positive or negative circumstance. Some unfavorable aerodynamic phenomena such as decambering and separation might happen at such working conditions, which inspired us to optimize the ducted fan configuration. One way to improve the blade performance is to generate a pre-whirled flow at the inlet for changing the flow angle. A design and optimization of an inlet guide vane (IGV) will be subsequently discussed in the next chapter.

4 Pre-Swirl At Inlet

4.1 Design Method of IGV

Figure 6 schematically illustrates the change of the inlet flow angle when the ducted fan are mounted with a pre-swirled IGV. It can obviously note that the rotor can work at

a positive attack angle with IGV.

A six-blade IGV is designed by multiple circular arc method, see in Figure 7. The projected meridional chord is 20 mm, the leading and trailing edge radius are 0.25 mm and 0.15 mm, respectively. The maximal thickness of the IGV blade is 1.5 mm and 15 mm away from the upstream rotor.

4.2 Aerodynamic Performance Comparison

The same numerical methodology as above has been applied on the ducted fan with a equipped IGV to predict its aerodynamics. Table 1 shows comparative performance parameters between the original lift fan model (M0) and modified model with IGV (M1) at design speed, it can be seen that the pre-whirl effect by the IGV increases the upstream rotor load and the total pressure ratio. For the upstream rotor, the efficiency and the thrust increased by 7% and 168%, respectively. Due to change in upstream rotor load, the flow conditions of downstream rotor changes as well, which leads to a slightly decline of pressure ratio, efficiency and thrust; in addition, the inlet guide vane creates negative thrust by 2.579 N. However, the pre-swirl effect caused by the IGV can enhance the aerodynamic performance of the lift fan. The entire thrust increased by about 10%, while the efficiency decreases by about 1.6% due to the low efficiency of the downstream rotor and aerodynamic loss of IGV.

4.3 Inlet/Outlet Flow Angle Analysis

A detailed inlet/outlet flow angle between the original lift fan and the modified one with IGV is shown in Figure 8. Figure 8(a) shows that the inlet flow angle increases around 10^o along with the spanwise position. At this moment, the majority of the blade working at a positive AOA which can product more lift corresponding to the results listed in Table 1. However, a negative effect caused by the IGV can be found in Figure 8(b) that the attack angle decreases compared with the original lift fan configuration which will decrease the aerodynamic performance of the downstream rotor.

In order to obtain a detailed understanding of the flow behavior inside the ducted fan, the static pressure contour on the blade surface as well as the IGV are plotted in Figure 9(a). It can be seen that the upstream rotor works at positive attack angle conditions due to the deceleration, pressure diffusion and stream guidance of IGV. Proper flow conditions were achieved for the upstream rotor, i.e. freedom from big separation means lower flow losses and correspondingly higher efficiency. The AOA and hence the blade load of R2 has declined as a result of the changed flow condition from R1, therefore, lower efficiency was observed for the fact that the proportion of frictional loss has increased ultimately.

The total pressure distribution was obtained at four different axial locations on S3 planes as in Figure 9(b). The total pressure ratio remains at the same level for the two rows of the rotor, which is beneficial for the reduction of gyroscopic torque. However, the boundary layers of both R1 and R2 are thick which can be seen on the S3 planes located right downstream of blades, therefore an increment of wake width and strength is to be expected as well as lower efficiency. In order to save the cost of design and manufacture, raw materials of PLA were used although it is weak in rigidity and strength. What becomes apparent is that the thickness of blades has to be increased, so do the profile losses and the flow drag, which must be paid much attention in further study.

4.4 Effect of Rotary Speed

Figure 10 shows the Speed characteristics comparison between the original lift fan and the modified lift fan with IGV. it can be found that: under different speed, the pressure ratio, axial thrust and power increase as the rotating speed increases both in original lift fan and the modified one. The total efficiency increases firstly and then decline along with the increasing rotating speed, where the maximum value peaks at 26000 rpm for the original one, and for the modified one, it is 22000 rpm that the efficiency achieve optimal. But for the original fan, the thrust or pressure ratio of rotor1 is about 1/3 of rotor2, which means the load of rotor1 is relatively smaller than expected. The thrust contribution of rotor1 is approximately equal to rotor2 for the modified lift fan, so it is with the pressure ratio, efficiency and power. In consideration of our goal of increasing the total thrust of the ducted fan, which determines whether the MAV could fly. It is beneficial for the contra-rotating fan to develop its performance better though the overall efficiency reduce a little after adding a row of IGV.

5 Conclusions

The paper conducted a numerical research on a 90mm diameter contra-rotating lift fan. The effect of axial space and speed are investigated. Due to the low thrust generated by this commercial ducted fan, an IGV has been parametrically designed to achieve a better thrust production which can guide our further design. The main conclusions are listed below:

(1) The axial space of the two blade rows significantly affect the overall aerodynamic performance. The mass flux, pressure ratio and axial thrust almost remain the same with the increasing axial space, while the efficiency firstly increases till 0.7c and then decreases.

(2) The reason of rotor1s poor working capacity has been revealed by analyzing the inlet/outlet and metal angles distribution along with the spanwise. A pre-swirl effect caused by rotor1 can enhance the aerodynamic performance.

(3) Equipping an IGV at the inlet of rotor1 makes a significant effect on the flow field, the efficiency of rotor1 increases by about 7%, and thrust increased by nearly 168%; even though the IGV creates a negative thrust of 2.759N, the total thrust increases by about 10%.

(4) The pressure ratio, axial thrust and power of both configurations (with/without IGV) increase as the increasing rotating. The total efficiency increases firstly and then declines along with the increasing rotating speed, where the maximum value peaks at 26000 rpm for the original one, and for the

Table 1: Performance Parameters Comparison of Original and Modified Design.

	$q_m(kg/s)$		π_k^*		Efficiency		Axial Thrust(N)		Power(kW)	
	M0	M1	M0	M1	M0	M1	M0	M1	M0	M1
IGV	\	\	\	0.993	\	\	\	-2.759	\	\
Rotor1	\	\	1.016	1.032	0.732	0.808	6.122	16.43	1.003	1.876
Rotor2	\	\	1.038	1.029	0.832	0.801	19.75	14.77	2.089	1.747
Total	0.554	0.581	1.055	1.060	0.797	0.781	25.87	28.44	3.091	3.623

modified one, it is 22000 rpm that the efficiency achieve optimal. The thrust contribution of rotor1 is approximately equal to rotor2 for the modified lift fan after adding an IGV, that means the IGV is beneficial for the contra-rotating fan to develop its performance better though the overall efficiency reduce a little.

ACKNOWLEDGEMENTS

The technical assistance from the NPU turbomachinery laboratory in providing the scanning geometry data is of great appreciated. This work has been financially supported by the National Natural Science Foundation of China [grant number 51376150]. All these supports are gratefully acknowledged.

REFERENCES

[1] T.G. Sylvester, R.J. Brown, and C.F. O'Connor. F-35b lift fan inlet development. In *AIAA Centennial of Naval Aviation Forum "100 Years of Achievement and Progress"*, 21-22, September 2011.

[2] G.P. Walker and D.A. Allen. X-35b stovl flight control law design and flying qualities. In *Biennial International Powered Lift Conference and Exhibit*, 5-7, November 2002.

[3] R.R. Harrington. *Full-Scale-Tunnel Investigation of the Static-Thrust Performance of a Coaxial Helicopter Rotor*. NACA TN-2318, New York, NY, 1951.

[4] I. Guerrero, K. Londenberg, P. Gelhausen, and A. Myklebust. A powered lift aerodynamic analysis for the design of ducted fan uavs. In *nd AIAA "Unmanned Unlimited" Systems, Technologies, and Operations*, 15-18, September 2003.

[5] M.H. Williams, J. Cho, and W.N. Dalton. Unsteady aerodynamic analysis of ducted fans. *Journal of Propulsion*, 7(5):800–804, 1991.

[6] G.S. Page. Design and analysis of single and dual rotation ducted fans. In *AIAA 34th Aerospace Sciences Meeting and Exhibit*, 15-18, Jan 1996.

[7] B.C. Stiltner et al. Detailed design, construction, and flight tests of a remotely piloted ducted fan mav. In *48th AIAA Aerospace Sciences Meeting Including the New Horizons Forum and Aerospace Exposition*, 4-7, Jan 2010.

[8] P. B. Sharama, Y. P. Jian, and D.S. Pundhir. Study of some factors affecting the performance of a contra-rotating axial compressor state. *Proceedings of the Institution of Mechanical Engineers, Part A: Power and Process Engineering*, 15(211), 1985.

[9] P. B. Sharama, Y. P. Jian, and D.S. Pundhir. Stalling behavior of a contra-rotation axial compressor stage. *ISABE*, 85(7087), 1985.

[10] Y. Wang, N. Niu, and B. Liu. two stage axial spacing of counter rotating compressor impact on performance. *Journal of Aerospace Power*, 25(3), 2010.

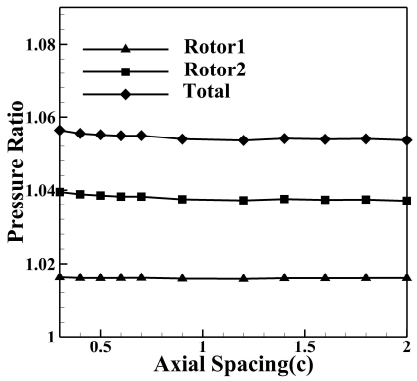

(a) Pressure ratio vs. axial space

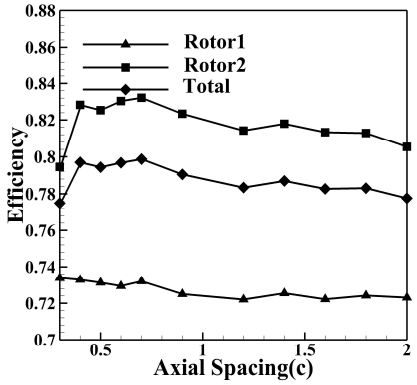

(b) Efficiency vs. axial space

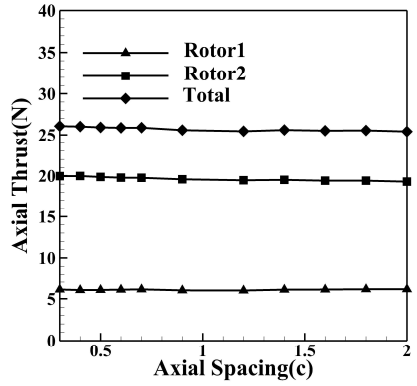

(c) Axial thrust vs. axial space

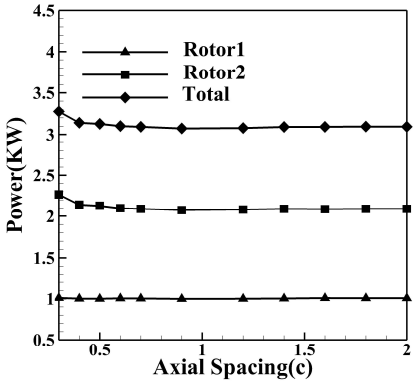

(d) Power vs. axial space

Figure 4: Aerodynamic performance of the axial space effect.

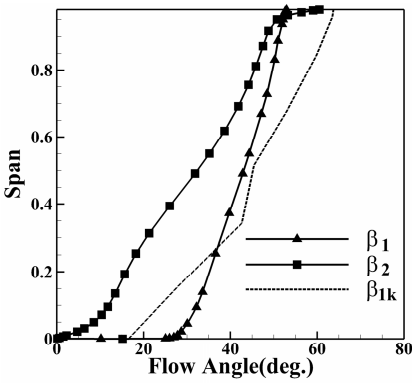

(a) Upstream rotor

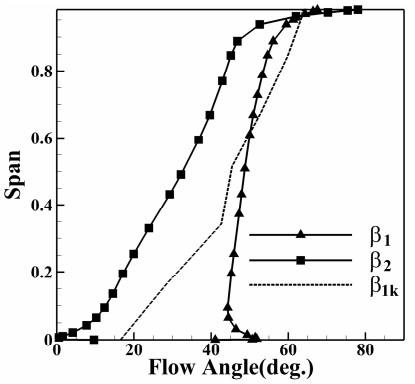

(b) Downstream rotor

Figure 5: The spanwise flow angle distribution.

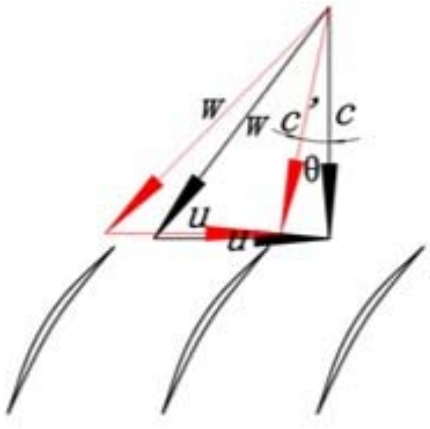

Figure 6: Velocity triangle comparison of rotor 1 at 50% span.

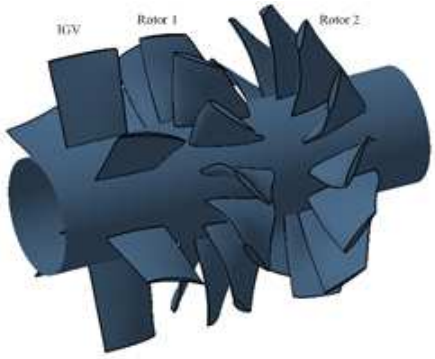

Figure 7: 3D configuration of the IGV mounted on the lift fan.

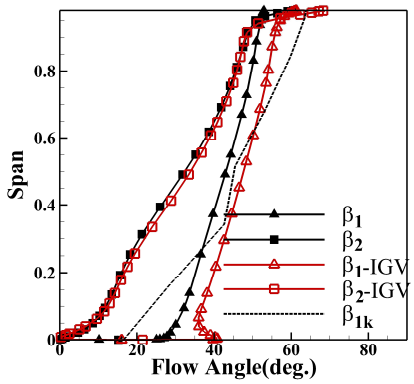

(a) Upstream rotor

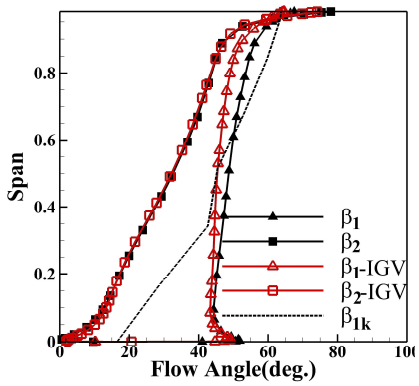

(b) Downstream rotor

Figure 8: The spanwise flow angle distribution.

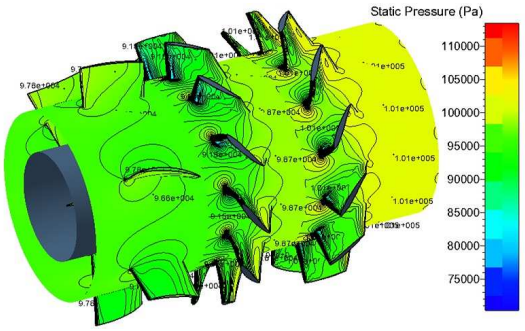

(a) Static pressure distribution

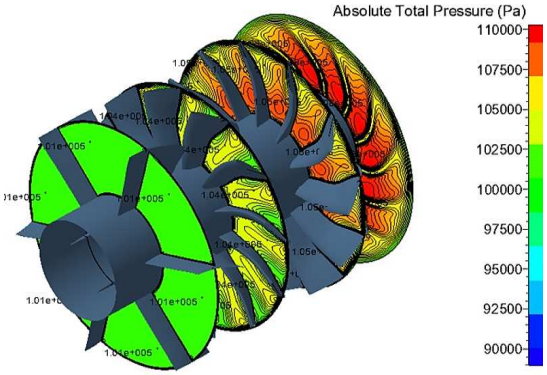

(b) Total pressure distribution on S3 planes

Figure 9: Pressure contour.

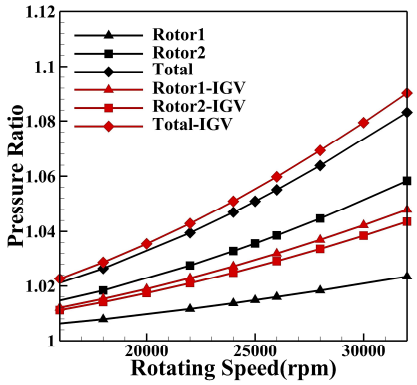

(a) Pressure ratio vs. RPM

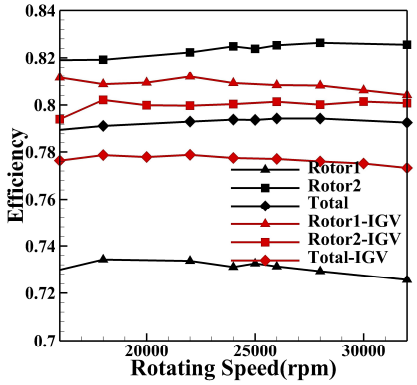

(b) Efficiency vs. RPM

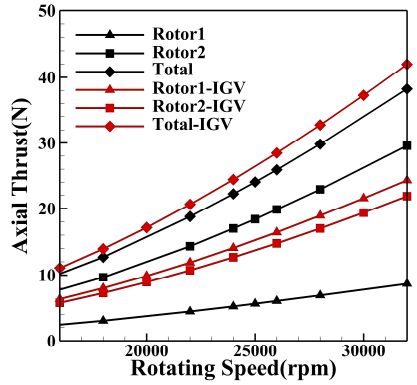

(c) Axial thrust vs. RPM

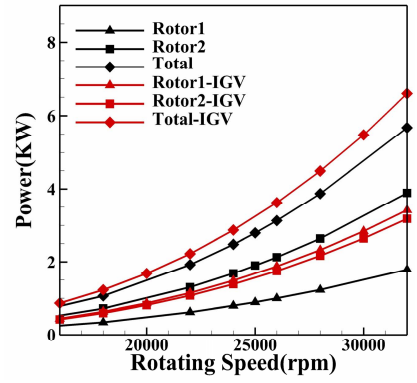

(d) Power vs. RPM

Figure 10: Speed characteristics comparison between original lift fan and modified lift fan with IGV.